frontiers in Physics

MINI REVIEW
published: 08 September 2020
doi: 10.3389/fphy.2020.00342

Budding and Fission of Membrane Vesicles: A Mini Review

Samo Penič[1]*, *Luka Mesarec*[1], *Miha Fošnarič*[2], *Lucyna Mrówczyńska*[3], *Henry Hägerstrand*[4], *Veronika Kralj-Iglič*[2,5] *and Aleš Iglič*[1,5,6]

[1] Faculty of Electrical Engineering, University of Ljubljana, Ljubljana, Slovenia, [2] Faculty of Health Sciences, University of Ljubljana, Ljubljana, Slovenia, [3] Department of Cell Biology, Institute of Experimental Biology, Adam Mickiewicz University, Poznań, Poland, [4] Cell Biology, Faculty of Science and Engineering, Åbo Akademi University, Åbo-Turku, Finland, [5] Institute of Biosciences and Bioresources, National Research Council, Naples, Italy, [6] Faculty of Medicine, University of Ljubljana, Ljubljana, Slovenia

In this mini-review, a brief historical survey of the mechanisms which determine the shapes of liposomes and cells and the budding and fission of their membrane is presented. Special attention is given to the role of orientational ordering of membrane components in thin membrane necks which connect the membrane buds (daughter vesicles) to the parent membrane. It is indicated that topological anti-defects in membrane necks may induce the rupture of the neck and the fission of the membrane daughter vesicles.

Keywords: vesiculation, vesicle fission, membrane ordering, membrane budding, topological defects

OPEN ACCESS

Edited by:
Francisco Monroy, Complutense University of Madrid, Spain

Reviewed by:
Aurora Hernandez-Machado, University of Barcelona, Spain
José Antonio Santiago, Metropolitan Autonomous University, Mexico

***Correspondence:**
Samo Penič
samo.penic@fe.uni-lj.si

Specialty section:
This article was submitted to Biophysics, a section of the journal Frontiers in Physics

Received: *19 March 2020*
Accepted: *22 July 2020*
Published: *08 September 2020*

Citation:
Penič S, Mesarec L, Fošnarič M, Mrówczyńska L, Hägerstrand H, Kralj-Iglič V and Iglič A (2020) Budding and Fission of Membrane Vesicles: A Mini Review. Front. Phys. 8:342. doi: 10.3389/fphy.2020.00342

1. INTRODUCTION

The main building block of the biological membranes is the lipid bilayer with embedded inclusions like proteins and glycolipids [1, 2]. Protein membrane inclusions may induce the local curvature changes of the membrane [3–5], resulting also in the global change of the cell shape [6–13]. The non-homogeneous lateral distribution [6–9, 14–16] and the phase separation of membrane inclusions (nanodomains) are important mechanism that may induce the local changes of membrane curvature and are therefore the driving force for transformations of the cell shape [12, 17–20]. The shapes of cells or lipid bilayer vesicles (as model systems) may also be changed by membrane skeleton or cytoskeleton forces [13, 19, 21–27]. Among them, the ATP consuming forces are very significant for sustaining different cell functions [12, 16, 28–32]. Consequently, new theoretical approaches for modeling the cell shape changes under the influence of the energy consuming active forces have recently been developed [12, 16, 28, 31, 32]. Until recently [29–31], it was also believed that the active forces are completely absent in the mechanisms of the determination of the RBC shape, when it was shown that NMIIA motor nanodomains may generate tension in the spectrin-F-actin RBC membrane skeleton and in this way partially control the RBC shape [29, 30] and the membrane vesiculation [31]. In accordance with experimental observations, it was shown [30] that myosin (NMIIA) motor nanodomains should be non-homogeneously distributed over the entire inner membrane surface of discocyte RBC. In addition, the normal component of the NMIIA nanodomain force should be different from zero and directed to the interior of the cell across the whole membrane surface, including the dimple region of the discocytic RBC, in order to keep the stable discocyte RBC shape and prevent a pancake shape transformation [30]. It should be pointed out that if NMIIA motor protein is contracted in the dimple region of the RBC, this may induce small local exvaginations and non-zero component of myosin force directed to the RBC interior. Because NMIIA motor nanodomains and actin molecules are distributed only on the inner membrane surface of RBC, the normal component of

the NMIIA motor nanodomain should be directed to the interior of RBC (inward). Experimental measurements of NMIIA densities at the dimple and rim of discocyte RBC shape confirmed the theoretical predictions of [30] that the NMIIA force density must be larger in the dimple than at the RBC rim in order to stabilize the discocyte RBC shape [30].

It was further shown that decreasing the difference between the relaxed areas of the outer layer and the inner lipid layer induces the inward bending of the RBC membrane [27, 33–36], while increasing the difference between the relaxed areas of the outer and inner membrane layers favors the outward bending [26, 27, 33–37]. In accordance, the exogenously added amphiphiles which predominantly bind in the outer lipid layer induce the transformation of the discoid RBC into the spiculated (echinocytic) RBC, while amphiphiles predominantly bound in the inner lipid layer induce the transformation into invaginated stomatocytic shapes [35, 36, 38]. RBC membranes have in addition to lipid bilayer also the membrane skeleton composed of the spectrin-F-actin network which is attached to the inner surface of the lipid bilayer [24]. It was indicated that besides the local and non-local bending energy [23, 39–47] also the shear elastic energy of the membrane skeleton [25–28, 33, 46] should be considered in the minimization of the membrane free energy to theoretically explain the observed stability of speculated (echinocytic) RBC shapes [25, 26]. It was also shown recently that in RBCs, the ATP-dependent membrane skeleton forces, exerted on the membrane by the skeleton nodes, may cause membrane softening, which influences the RBC deformability to facilitate the movement of RBCs through narrow capillaries [28].

2. MEMBRANE BUDDING AND ENDOVESICULATION

The membrane skeleton of RBC plays an important role also in the vesiculation of the RBC membrane [35, 37, 48–51]. Because of the local disruption of the interactions between the membrane skeleton and the membrane bilayer [48], the RBC microexovesicles are depleted in the membrane skeleton [49]. It was shown that at sublytic concentrations of amphiphiles in the RBC suspension, the anisotropic amphiphiles induce tubular membrane budding and the release of stable tubular microexovesicles [18, 35, 37, 49, 51], while most of the other amphiphile molecules induce small, predominantly spheroidal microexovesicles that are formed from small membrane buds [8, 35, 51, 52]. The experimentally observed tubular budding and vesiculation of the RBC membrane [18, 35, 49, 51] can be theoretically explained by deviatoric membrane properties due to the in-plane orientational ordering of anisotropic membrane inclusions [8, 10, 15, 53–61].

Certain amphiphilic molecules can induce stomatocyte shape transformation and the formation of a large number of small spheroidal membrane invaginations (buds/endovesicles) in the region of large stomatocytic invagination [35, 36]. But it is also possible that small exvaginations are formed in the region of large stomatocyte invaginations. For example, it was observed in RBCs that the lipid rafts component ganglioside GM1 distributes and even enriches the membrane of large stomatocytic RBC invaginations [17]. It was proposed that single GM1 molecules have zero intrinsic curvature, while small GM1 aggregates have the positive intrinsic curvature [62]; therefore, it is possible that small GM1 aggregates in the region of large stomatocyte invagination(s) also induce the outward budding and the release of small exovesicles which, however, can hardly be observed in *in vitro* experiments since they are washed out in the preparation of the samples for microscopy. It was pointed out that the recently suggested role of active forces of NMIIA motors [29] in the RBC membrane shape determination [30] may play an important role also in membrane endovesiculation and the control of the shape and size of membrane endovesicles [31]. By using Monte Carlo (MC) simulations, it was indicated that the formation of a large number of small spheroidal membrane buds/endovesicles may be coupled to non-homogeneous lateral distribution active forces motor nanodomains/inclusions and to a global invaginated closed membrane shape transformation [31].

The main subject of this mini-review is the possible theoretical explanation of the fission of membrane endovesicles [i.e., the rupture of the neck connecting the membrane buds (daughter vesicles) with the parent membrane] following the formation of membrane invagination/buds. Our interest in the subject was motivated by experimental observations of a large number of buds/endovesicles in red blood cells (RBCs) [35, 36] (**Figure 1**) and by the results of Monte Carlo (MC) simulations (**Figure 2**).

Figure 1 shows transmission electron microscopy (**Figure 1A**) and confocal laser scanning microscopy images (**Figure 1B**) of a large number of small inward membrane buds/endovesicles in an invaginated stomatocytic RBC induced by amphiphilic molecules of chlorpromazine hydrochloride. Small spheroidal buds/endovesicles shown in **Figure 1** are concentrated in the vicinity of the large primary invagination(s) of stomatocytic RBCs [17, 63].

Figure 2 shows the MC simulations predicted closed membrane shape with the membrane inclusions (nanodomains) with the negative intrinsic curvature which may induce the formation of long undulated thin inward membrane protrusions (buds). The inclusions are accumulated in the region of the protrusions. The theoretically predicted shapes in **Figure 2** may partially correspond to situations in RBCs when the protrusion is growing in the region where the local disruption of the interactions between the membrane skeleton and the membrane bilayer appears or the skeleton is detached from the protrusion [48, 49], so that the inward membrane protrusion is not covered by membrane skeleton.

Figure 2 also shows the cluster size distributions that were determined from the averaging over the convergent MC realizations. It can be seen in **Figure 2** that the cluster size distribution of nanodomains/inclusions has only two peaks corresponding to two, spheroidal and necklace-like aggregate of inclusions in the form of protrusions (phase separation). We may conclude that the inclusions aggregates into curved membrane protrusions or buds which is the consequence of non-zero (negative) intrinsic curvature of inclusions and high enough interaction (attractive) energy between inclusions.

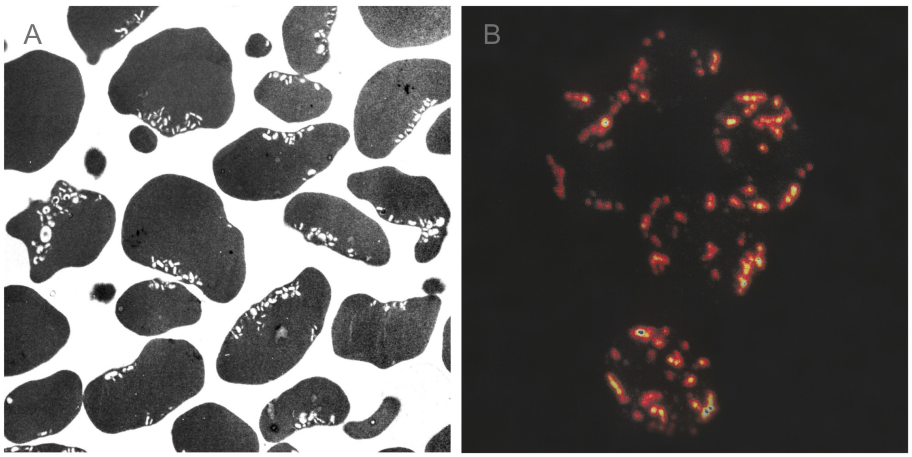

FIGURE 1 | Transmission electron micrograph **(A)** and confocal laser scanning microscopy of invaginated stomatocytic RBC incubated with amphiphilic molecules chlorpromazine **(B)**. Chlorpromazine molecules induce the formation of a large number of small membrane buds/endovesicles. Adapted from Hägerstrand et al. [17] and Bobrowska-Hägerstrand et al. [63].

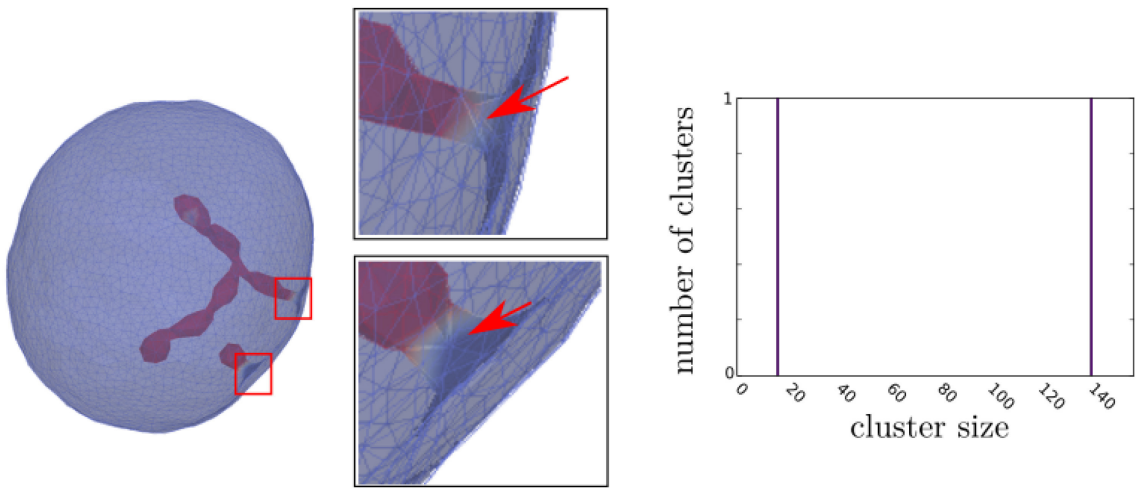

FIGURE 2 | The Monte Carlo simulation of the RBC membrane transformation induced by mobile membrane inclusions with intrinsic curvature $c = -1\,\mathrm{d}_{\mathrm{min}}^{-1}$. Concentration of membrane inclusions $p = 5\%$. The triangulated membrane surface is drawn semitransparent to uncover its interior shape. Red arrows in enlarged insets point to the neck area, where there is a lack of inclusions. In the corresponding cluster-size distributions, the y-axis is the ensemble averaged number of inclusion clusters of each size and the x-axis is the inclusion cluster size. The values of other model parameters are: local bending stiffness of lipid bilayer $\kappa = 25\,\mathrm{kT}$ and direct interaction parameter $w = 1.25\,\mathrm{kT}$. The parameters for simulations are based on values in [31]. The simulations were run on a personal computer with Intel i7-7500U processor and 8 GB of RAM; however, the memory requirements for the Monte Carlo simulations are not the limiting factor for the speed of computations. Each simulation was running on a single thread, where simulations with multiple parameter sets were executed on the same processor. The average time for simulations to complete 1,000 time-steps with $100 \cdot 10^3$ mcs each was ≈ 14.5 days. After finishing the simulations, the graph of free energy term and asphericity was observed to check if thermal equilibrium was reached.

The MC program and theoretical basis used in calculations presented in **Figure 2** were described in details elsewhere [16, 31]. For simulations, we used `trisurf_ng`, a software we developed ourselves. It performs random thermal fluctuations based on Metropolis-Hastings Monte Carlo algorithm and it is described in literature [5, 16, 64, 65]. The model for the discretization of a closed surface representing a phospholipid vesicle is a triangulated mesh, consisting of vertices, connected with bonds, forming triangles on the surface. The number of vertices used in simulation was $N = 3,127$. The initial state of the triangulated surface is a pentagonal dipyramid with all the edges divided into equilateral bonds so that the network is composed of $3(N-2)$ bonds forming $2(N-2)$ triangles. The phospholipid membrane and vertices representing the membrane have no intrinsic curvature ($c_0 = 0$), except for N_c randomly selected vertices with inclusions that were given non-zero isotropic intrinsic curvature of $c_0 = -1\,d_{\mathrm{min}}^{-1}$, where d_{min} is the minimal distance between the vertices in triangulated mesh and can be

used as a dimensional scaling parameter. The positive curvature means the membrane will locally bend toward the exterior, the negative curvature will force the membrane to locally bend toward the interior of the vesicle [16, 31]. The energy is a sum of two components: $W = W_b + W_d$, where W_b is the bending energy of the membrane and W_d is the energy of the direct interaction between vertices with intrinsic curvature. For the bending energy W_b of the membrane, the standard Helfrich expression [66] for a tensionless membrane including a term that represents the intrinsic curvature is used. The contribution of the Gaussian curvature to the change of bending energy is omitted from the expression $W_b = \frac{\kappa}{2} \oint_A (c_1 + c_2 - c_0)^2 \, \mathrm{d}A$, where κ is the bending stiffness of the membrane, c_1, c_2, and c_0 are the two principal curvatures and the intrinsic curvature of the vesicle membrane at the point under consideration. The integration is performed over membrane area A. In **Figure 2**, we adopted the value of κ which is compatible with the membrane of giant lipid vesicles [67, 68]. In the absence of inclusions with attraction forces (direct interactions) between them, our simulations can produce spherical shape, a discocyte biconcave shape and also pure stomatocyte shape transformation (without small membrane invaginations) after proper variation of the model parameters [69]. For modeling attraction force between the vertices with intrinsic curvature, the additional energy term was used [16, 31]: $W_d = -w \sum_{i<j} \mathcal{H}(r_0 - r_{ij})$, where w is a direct interaction constant, defining the affinity for the inclusions to group into rafts. The energy is summed over all inclusion pairs with their in-plane distance r_{ij}, where $\mathcal{H}(r)$ is a Heaviside step function and r_0 is the range of direct interaction. The value for direct interaction distance is limited to neighboring nodes with inclusions ($r_0 = d_{\max}$). In MC simulations [16, 31] presented in **Figure 2**, we do not consider explicitly the bilayer structure of the membrane lipid bilayer. Also the skeleton elasticity is not explicitly taken into account. Therefore, we took the value of the bending modulus which is compatible with the membrane of giant lipid vesicles [67, 68] and not with the RBC membrane [28, 70–73]. Further, for simplicity reasons, in the current MC simulations we consider membranes with only one type of inclusions that can induce local membrane bending due to their negative intrinsic curvature [16, 31].

Due to the simplifications introduced in our MC model, we cannot perform a detailed comparison of the predictions of MC simulations and experimentally observed amphiphile induced large membrane invagination(s) in the RBCs accompanied by the formation of a large number of small membrane invaginations, i.e., buds/endovesicles [17, 63], as shown in **Figure 1**. As written above, we hope that further improvements of the MC model presented in this work will allow us to better understand the phenomena presented in **Figure 1** and other processes connected to exo- and endo-vesiculation in RBCs. Among others also the active forces in the RBC membrane which are generated by NMIIA motor nanodomains (inclusions) bound to F-actin of the RBC membrane skeleton [29–31]. Previous theoretical descriptions of the invaginated (stomatocyte) shape, based on the minimization of the membrane bending energy, were able to explain only large stomatocyte invagination(s), but not also the large number of small membrane buds and endovesicles. Accordingly, it was shown recently [31] that the formation of invaginations/buds may be coupled also to a global shape transformation driven by the non-homogeneous lateral distribution of active force. It was indicated that the invaginated stomatocytic shapes can have different forms of invaginations [31], which is an extension of the previously theoretically predicted shape classes of the invaginated stomatocytic shapes which were mostly limited to the simple stomatocytic shape with one or two large smooth invaginations (see for example [27, 44]), as was experimentally observed also in a giant unilamellar lipid vesicle [74]. Active force nanodomains/inclusions may induce the formation of a large number of small membrane invaginations/buds on the large stomatocyte invagination [31].

3. FISSION OF THE MEMBRANE DAUGHTER ENDOVESICLES

Long undulated membrane protrusions as predicted by MC simulations in **Figure 2** may be further transformed into small independent spherical buds/endovesicles, due to the frustrations in the orientational ordering of membrane components in the highly curved membrane necks (**Figure 3**). The same mechanism can also be responsible for the possible detachment of the complete inward membrane protrusion from the parent membrane [75] and the consequent formation of the buds/endovesicles (**Figure 1**).

We shall describe below that topological anti-defects may induce the rupture of the highly curved membrane structures possessing the in-plane orientational ordering of membrane components. Biological membranes may exhibit global and local in-plane orientational ordering [51, 75–77]. A lipid bilayer is basically a thin liquid crystal film [66, 77]. The orientational order in membranes could occur due to the anisotropic shape of membrane components like anisotropic proteins or lipids [8, 53, 56, 78–80]. A typical example of inclusions possessing nematic order [58] are anisotropic banana shaped BAR protein domains [11, 81, 82]. The orientational order often arises in highly curved parts of the membrane due to the alignment of these anisotropic components [8, 51, 76]. Furthermore, chiral membrane constituents [83, 84] or self-organized filament networks [85] may also be a source of the membrane orientational order. The orientational order in membranes has been observed in giant unilamellar vesicles where lipid molecules were in the gel or in some other ordered phase [58, 76, 86]. In-plane ordering in biological membranes may occur also due to the tilt of lipid tails relative to the surface normal [83, 87, 88].

In biological membranes possessing the tangential (in-plane) orientational ordering, topological defects are often present. Furthermore, topological defects are, in most cases, unavoidable due to topological reasons [89, 90]. Below, we shall describe the possible mechanism of the fission of the single membrane invagination/bud and the fission of the necklace-like buds/endovesicles predicted by MC simulations and indicated in *in vitro* experiments (**Figure 1**), where we shall take into account the possible role of topological defects in highly curved regions of the RBC membrane necks [60, 75]. Topological defects are a source of relatively large local elastic penalties. At the

origin of defects, the ordering field is melted [91, 92], which is why the presence of defects might have a strong impact on systems' properties. Topological defects in biological membranes could for example trigger significant biological processes, such as cell membrane fission or fussion [75, 93]. Below, we will demonstrate how topological defects might trigger the pinching-off of the large and small membrane invaginations/buds from the parent membrane (membrane fission) and the fission of the necklace-like buds/endovesicles in membranes exhibiting in-plane nematic ordering.

4. MODELING OF MEMBRANE ORDERING IN THE NECK REGION

Biological membranes may exhibit global or local in-plane orientational ordering [51, 75–77]. Here, we shall describe the application of a simple 2-D Landau-de Gennes type model to qualitatively demonstrate the assembly of topological antidefects in regions with the high negative Gaussian curvature (membrane necks). Strong orientational order in membranes often arises in highly curved parts [8, 51, 76]. Therefore, for simplicity reasons, we assume in our simulations that nematic ordering is present only in the catenoid-like neck region of the membrane. Surface patches with the positive (negative) Gaussian curvature have a tendency to host topological defects (antidefects) [75, 94–96]. If the Gaussian curvature is strong enough, it can even trigger the formation of new defect-antidefect pairs. The presence or the formation of a topological defect (antidefect) in a surface patch with the positive (negative) Gaussian curvature neutralizes that surface patch in terms of "effective topological charge" as described in [94]. Simulations of orientational ordering on catenoid necks, which are geometrically the same as the membrane necks in our paper, show that antidefects assemble in catenoid necks, even though these necks are not connected to the rest of the membrane surface [97]. Therefore, we expect topological antidefects to assemble in the neck regions also if there is no or very weak orientational order and in the other regions of the membrane, as is actually the case in the RBC membrane.

Orientational (nematic) ordering is studied on catenoid-like membrane neck surfaces. Molecules which contribute to orientational ordering are bound to lie on the local tangent plane on a surface. Local surface curvature is described by the principal curvatures c_1 and c_2. Gaussian curvature, which acts as an attractor for topological defects, is defined as: $K = c_1 c_2$. In order to describe the orientational nematic ordering on a closed surface, we introduce a surface order tensor $\mathbf{Q}$, which can be expressed in its diagonal form as [90, 98]:

$$\mathbf{Q} = \lambda(\mathbf{n} \otimes \mathbf{n} - \mathbf{n}_\perp \otimes \mathbf{n}_\perp). \quad (1)$$

Here, $\otimes$ represents a tensor product and $\{\mathbf{n}, \mathbf{n}_\perp\}$ are the eigenvectors of $\mathbf{Q}$ corresponding to the eigenvalues of $\{\lambda, -\lambda\}$ [94, 99]. In Equation (1), $\mathbf{n}$ represents the nematic director field, i.e., the direction of molecules, which exhibits head-to-tail invariance [92]. On two-dimensional surfaces, the topological charge is the same as the winding number, which is calculated as the total rotation of the orientational field $\mathbf{n}$ divided by 2π upon encircling the defect core counter-clockwise [91, 92, 100]. The topological charge of topological defects/antidefects is positive/negative. Furthermore, the amplitude λ represents the degree of orientational order, where the upper bound ($\lambda = 1/2$) corresponds to the maximal degree of the orientational order, while the lower bound ($\lambda = 0$) represents the isotropic state, where the orientational order is lost. Consequently, the points on the surface exhibiting $\lambda = 0$ usually signal topological defects, since at the core of topological defects the orientational order is melted [90, 94]. Furthermore, topological defects also display a singularity in $\mathbf{n}$ in the center of their core [94].

The total free energy associated with nematic in-plane ordering in the membrane is given as [90, 94, 98]:

$$F_{\text{tot}} = \int\int_{\zeta} \left(-\alpha \, Tr\mathbf{Q}^2 + \frac{\beta}{2} \left(Tr\mathbf{Q}^2 \right)^2 + \frac{k_\text{i}}{2} \left| \nabla_\text{s} \mathbf{Q} \right|^2 \right) d^2\mathbf{r}, \quad (2)$$

where ∇_s stands for the surface gradient operator, $d^2\mathbf{r}$ is an infinitesimal surface element and the integration is carried out over the whole membrane neck surface area ζ. The first two terms in Equation (2) represent the condensation term, which enforces the equilibrium nematic ordering amplitude $\lambda_0 = \sqrt{\alpha/\beta}$, where α and β are positive material constants [94]. The third term in Equation (2) is the orientational elastic term and is weighted by the positive intrinsic k_i elastic constant [94]. This term represents the direct interactions between neighboring molecules, i.e., the energy associated with this term is minimized if the neighboring molecules are parallel. Furthermore, the nematic order correlation length, i.e., the characteristic material-dependent length of the model, is expressed as $\xi = \sqrt{k_\text{i}/\alpha}$ [90, 94].

Orientational ordering configurations were calculated on the necks of fixed closed membrane surfaces. For demonstration purposes, we chose two types of shapes, i.e., invaginated stomatocyte (cup-shaped) shapes and necklace-like endovesicle shapes (similar to invaginated bud presented in **Figure 2**). Both types of shapes exhibit a region with the negative Gaussian curvature, which acts as an attractor for topological antidefects [75, 94–96]. On neck surfaces of these fixed shapes, equilibrium nematic ordering configurations are determined by minimizing the free energy associated with nematic ordering (Equation 2). The minimization is performed using the Monte Carlo method. In the minimization procedure, the equilibrium profiles of nematic ordering amplitude λ and the nematic director field $\mathbf{n}$ in the neck region of the membrane ζ are determined. Further numerical details are described in [94].

5. DISTRIBUTIONS OF ANTIDEFECTS IN MEMBRANE NECK REGIONS

In **Figures 3**, **4**, it is shown how topological antidefects can cause fission of a closed membrane into two separate closed membrane surfaces. In our simulations, we calculated the orientational ordering in the neck regions on necklace-like buds/endovesicles (**Figure 3**) and in the neck regions of invaginated (stomatocyte) membranes (**Figure 4**) with different

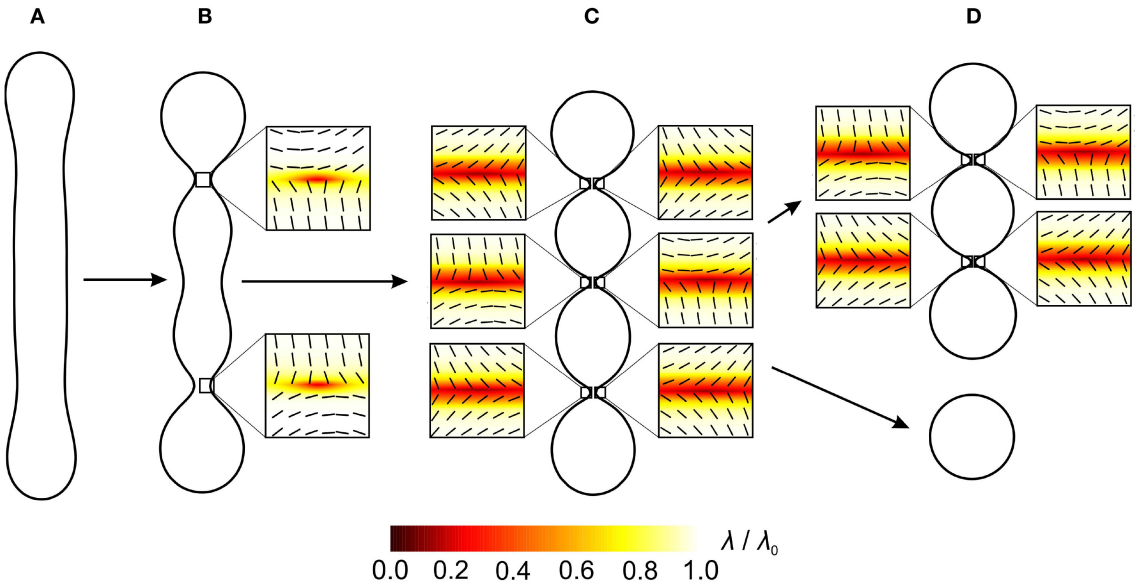

FIGURE 3 | Necklace-like buds/endovesicles with topological antidefects in their necks. The sequence demonstrates the transformation from the shape without a prominent neck **(A)** through the intermediate shape **(B)** to the shape with three prominent thin necks **(C)**. Finally, the neck rupture results in the formation of two distinct membranes **(D)**. The positions of antidefects are marked by small squares. Orientational ordering profiles with the superimposed nematic director fields in the vicinity of topological antidefects are magnified. $R/\xi = 21$, where R represents a typical linear dimension of a shape and ξ the nematic order correlation length defined in section 4.

neck radii. The color plot in **Figures 3**, **4** represents the nematic ordering amplitude, while the nematic director field (i.e., the orientation of molecules) is denoted by thin lines. At the core of topological defects/antidefects, the nematic order is lost [90, 94, 99]. Therefore, topological defects (and antidefects) are located at the points on the surface exhibiting $\lambda = 0$. The approximate positions of topological antidefects in thin membrane necks are schematically shown in **Figures 3**, **4**—they are marked by small squares. In these figures, orientational ordering profiles in the vicinity of topological antidefects are magnified.

In **Figure 3**, we analyse how topological antidefects assemble in the neck region when the neck gets thinner. The shape in **Figure 3A** does not have a prominent neck, therefore, it does not host any antidefects. The shape in **Figure 3B** hosts two $m = -1/2$ antidefects, and the shape in **Figure 3C** hosts six $m = -1/2$ antidefects. As the necks are getting thinner, more and more $m = -1/2$ antidefects assemble in the neck regions with the negative Gaussian curvature. The fact that the positive (negative) Gaussian curvature (deviatoric curvature) acts as an attractor for topological defects (antidefects) is well-established [75, 94–96].

A similar phenomenon is observed in **Figure 4**. The shape in **Figure 4A** hosts no topological antidefects because the negative Gaussian curvature in the neck is not strong enough. The shape in **Figure 4B** hosts two $m = -1/2$ antidefects and the shape in **Figure 4C** hosts four $m = -1/2$ antidefects. As the neck of the invaginated membrane region becomes thinner, more and more $m = -1/2$ antidefects assemble in the neck region. The neck region has the negative Gaussian curvature and acts as a strong attractor for antidefects [75, 94–96]. Consequently, this triggers the formation of new antidefects in the neck region. Note that four $m = -1/2$ antidefects in the neck region represent a limit case scenario in which the catenoid-like neck structure is neutral in terms of the "effective topological charge" as described in [94], i.e., the real topological charge of antidefects neutralizes the so-called smeared curvature topological charge of a catenoid surface [94]. Four $m = -1/2$ antidefects on a highly curved catenoid-like neck surface are therefore topologically favorable [97], while there is no topological reason for more antidefects to occur in the membrane neck.

In both cases (**Figures 3**, **4**), antidefects assemble in the neck regions as the necks get thinner. Topological defects/antidefects are a source of large local elastic penalties. At the core of topological defects and antidefects, the ordering field is melted and the degree of nematic ordering is relatively weak [91, 92]. In **Figure 3C**, two antidefects are located within each neck, while in **Figure 4C**, the neck region of invaginated stomatocyte hosts 4 antidefects. In both cases, neck regions represent relatively small surface areas, which host many topological antidefects. Consequently, local interactions between neighboring molecules within the neck regions are weakened, which might result in the neck rupture, leading to the fission process [75]. This process is shown in **Figures 3D**, **4D**, where two distinct closed membranes are formed. In **Figure 4D**, the neck rupture results in the formation of a closed membrane surface inside another closed membrane surface. In both cases, there is no more need for antidefects after the fission process because there is no more neck with strong negative Gaussian curvature (i.e., large curvature deviator).

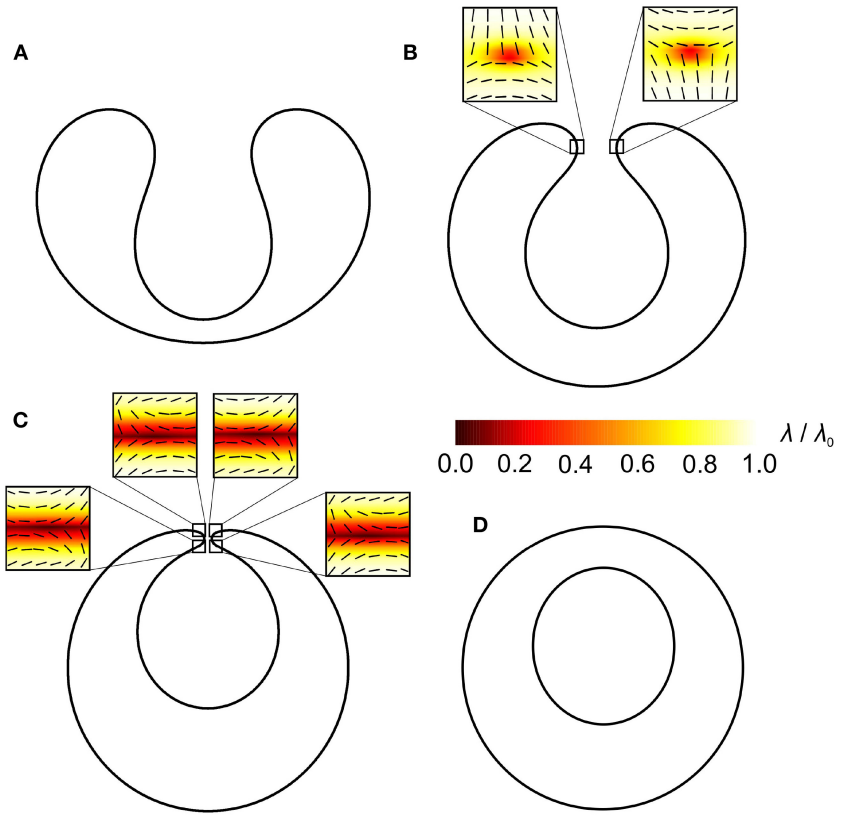

FIGURE 4 | Invaginated stomatocytes with topological antidefects in their neck region. The sequence demonstrates the transformation from a relatively opened stomatocyte **(A)** through the intermediate stomatocyte **(B)** to the stomatocyte with a thin neck **(C)**. Finally, the stomatocyte neck rupture results in the formation of one closed membrane surface inside another **(D)**. The positions of antidefects are marked by small squares. Orientational ordering profiles with the superimposed nematic director fields in the vicinity of topological antidefects are magnified. $R/\xi = 21$, where R represents a typical linear dimension of a shape and ξ the nematic order correlation length defined in section 4.

6. WHY THE GAUSSIAN TERM IN HELFRICH LOCAL BENDING ENERGY CANNOT EXPLAIN VESICLE FISSION

As pointed out by [101], in lipid bilayer vesicle, the daughter vesicle remains connected to the mother vesicle by microscopic neck after budding. It was also suggested that in the case of one-component giant unilamellar lipid vesicles (GUVs), the neck connecting the daughter to the mother vesicle may be stabilized by lateral segregation of membrane components, i.e., by the accumulation of impurities in the neck having high deviatoric curvature, which decreases the membrane free energy [102]. It was later shown that the accumulation of anisotropic membrane components can actually decrease the membrane free energy and stabilize a thin microscopic neck between the mother and the daughter vesicle [8, 61].

The neck can be additionally stabilized by the orientational ordering of lipids themselves in the deviatoric curvature region of the neck [76]. It was shown also in cellular systems, experimentally and theoretically, that the neck can also be elongated in the nanotube that connects the daughter to the mother part of the vesicle [61, 103]. In GUVs, such lipid nanotubes are usually invisible because they are too thin to be observed [104, 105]. After the breaking of the neck (i.e., fission) and the formation of a spherical mother and a (inner or outer) daughter vesicle, the decrease of the membrane free energy due to the orientational ordering of anisotropic membrane components is no longer present. Therefore, the orientational deviatoric free energy increases after the fission, i.e., the fission is not favored by the deviatoric (orientational ordering) energy.

Furthermore, it was indicated by [55] that in the case of homogeneous isotropic and thin membrane, there is essentially no obvious physical reason why the mother and the daughter vesicle, connected by a microscopic neck, would have smaller Helfrich bending energy after fission and a decrease in this energy by $|4\pi k_G|$ (where k_G is the Gaussian bending constant/modulus) just because of the change of topology after fission and disappearance of a microscopically small neck. Therefore, we suggest that a possible driving force of the fission process might be topological defects in the region (vicinity) of the neck due to high orientational ordering of anisotropic membrane components [8]. When the topological defect disappears, the energy might be reduced to a large extent due to the change

of the direct interaction energies between the molecules in the topological defect/antidefect.

Note also that in highly curved membrane parts, the so-called extrinsic $(c_1^2 - c_2^2)\cos(2\omega)$ [60, 97, 106] or deviatoric $(c_1 - c_2)\cos(2\omega)$ [51, 76] curvature term might play an important role. Here, ω describes the orientation of the membrane component (inclusion) in the principal axis system. It was shown in [97] that taking into account the extrinsic term would only affect the local spatial distribution of antidefects within the necks—it would not change the fact that topological antidefects assemble in the neck region. Without the extrinsic term, topological antidefects are assembled at the equatorial ring of the neck, where the Gaussian curvature exhibits the minimal value as demonstrated in this paper. If we take into account the extrinsic term, topological antidefects are expelled from the equatorial ring because of strong extrinsic ordering field [97]. Nevertheless, in this case, topological antidefects assemble near the equatorial ring of a neck. Topological antidefects are therefore robustly present within or very near the equatorial ring of a neck [97].

The incorporation of additional types of membrane inclusion in our model would also connect the mechanisms of formation of the isotropic inclusions enriched protrusion and the anti-defects driven disruption of the neck connecting the bud and the parent membrane. The consideration of additional anisotropic inclusions in the MC model would provide the missing mechanism of the growing/stabilization of the neck between the bud and the parent membrane driven by the accumulation of anisotropic membrane components/inclusions [8, 61, 76, 101, 102]. In the present work, we considered only isotropic inclusions with the negative intrinsic curvature which are depleted from the necks connecting the membrane protrusions/buds to the parent membrane, as can be clearly seen in **Figure 2**.

7. CONCLUSIONS

It is shown in this paper that the topological anti-defects may be created in the membrane necks if the thickness of the neck is small enough. It is further proposed that topological anti-defects in thin membrane necks, which connect the membrane buds (daughter vesicles) to the parent membrane, may induce the rupture of the neck and thus the fission of the membrane daughter vesicles. On the other hand, the formation of the neck is facilitated and energetically favored by orientational ordering and the accumulation of the anisotropic membrane components in the neck. This means that both processes, i.e., the formation and the thinning of the membrane neck, as well as the rupture of the neck are driven by the same mechanisms, i.e., orientational ordering and the accumulation of anisotropic membrane components in the neck.

AUTHOR CONTRIBUTIONS

AI, VK-I, and HH initiated this study. SP wrote the Monte Carlo program and prepared MC figures. MF amended the numerical procedures in the MC program and produced the MC results. HH and LMr prepared the experimental figures. LMe calculated the nematic profiles in the neck regions. AI, VK-I, SP, HH, LMr, and LMe wrote the manuscript. All authors contributed to the article and approved the submitted version.

FUNDING

This project has received funding from the European Union's Horizon 2020 research and innovation programme under grant agreement no. 801338 (VES4US project) and from the grant nos. P2-0232, P3-0388, J1-9162, and J2-8166 from the Slovenian Research Agency (ARRS).

REFERENCES

1. Cevc G, Marsh D. *Phospholipid Bilayers: Physical Principles and Models*. New York, NY: Wiley (1987).
2. Israelachvili JN. *Intermolecular and Surface Forces*. London: Academic Press (1997).
3. Szleifer I, Kramer D, Ben-Shaul A, Gelbart WM, Safran SA. Molecular theory of curvature elasticity in surfactant films. *J Chem Phys*. (1990) **92**:6800–17. doi: 10.1063/1.458267
4. Nielsen C, Goulian M, Andersen OS. Energetics of inclusion-induced bilayer deformations. *Biophys J*. (1998) **74**:1966–83. doi: 10.1016/S0006-3495(98)77904-4
5. Fošnarič M, Bohinc K, Gauger DR, Iglič A, Kralj-Iglič V, May S. The influence of anisotropic membrane inclusions on curvature elastic properties of lipid membranes. *J Chem Inform Model*. (2005) **45**:1652–61. doi: 10.1021/ci050171t
6. Markin V. Lateral organization of membranes and cell shapes. *Biophys J*. (1981) **36**:1–19. doi: 10.1016/S0006-3495(81)84713-3
7. Leibler S. Curvature instability in membranes. *J Phys*. (1986) **47**:507–16. doi: 10.1051/jphys:01986004703050700
8. Kralj-Iglič V, Heinrich V, Svetina S, Žekš B. Free energy of closed membrane with anisotropic inclusions. *Eur Phys J B Condens Matter Complex Syst*. (1999) **10**:5–8. doi: 10.1007/s100510050822
9. Iglič A, Babnik B, Bohinc K, Fošnarič M, Hägerstrand H, Kralj-Iglič V. On the role of anisotropy of membrane constituents in formation of a membrane neck during budding of a multicomponent membrane. *J Biomech*. (2007) **40**:579–85. doi: 10.1016/j.jbiomech.2006.02.006
10. Walani N, Torres J, Agrawal A. Endocytic proteins drive vesicle growth via instability in high membrane tension environment. *Proc Natl Acad Sci USA*. (2015) **112**:E1423–32. doi: 10.1073/pnas.1418491112
11. Mesarec L, Góźdź W, Iglič VK, Kralj S, Iglič A. Closed membrane shapes with attached BAR domains subject to external force of actin filaments. *Colloids Surfaces B*. (2016) **141**:132–40. doi: 10.1016/j.colsurfb.2016.01.010
12. Gov N. Guided by curvature: shaping cells by coupling curved membrane proteins and cytoskeletal forces. *Philos Trans R Soc B Biol Sci*. (2018) **373**:20170115. doi: 10.1098/rstb.2017.0115
13. Discher DE. Biomembrane mechanical properties direct diverse cell functions. In: Bassereau P, Sens P, editors. *Physics of Biological Membranes*. Basel: Springer (2018). p. 263–85. doi: 10.1007/978-3-030-00630-3_11
14. Fošnarič M, Iglič A, May S. Influence of rigid inclusions on the bending elasticity of a lipid membrane. *Phys Rev E*. (2006) **74**:051503. doi: 10.1103/PhysRevE.74.051503
15. Mesarec L, Góźdź W, Kralj S, Fošnarič M, Penič S, Kralj-Iglič V, et al. On the role of external force of actin filaments in the formation of tubular protrusions of closed membrane shapes with anisotropic membrane components. *Eur Biophys J*. (2017) **46**:705–18. doi: 10.1007/s00249-017-1212-z
16. Fošnarič M, Penič S, Iglič A, Kralj-Iglič V, Drab M, Gov N. Theoretical study of vesicle shapes driven by coupling curved proteins and active cytoskeletal forces. *Soft Matter*. (2019) **15**:5319–30. doi: 10.1039/C8SM02356E

17. Hägerstrand H, Mrówczyńska L, Salzer U, Prohaska R, Michelsen KA, Kralj-Iglič V, et al. Curvature-dependent lateral distribution of raft markers in the human erythrocyte membrane. *Mol Membr Biol*. (2006) **23**:277–88. doi: 10.1080/09687860600682536
18. Iglič A, Lokar M, Babnik B, Slivnik T, Veranič P, Hägerstrand H, et al. Possible role of flexible red blood cell membrane nanodomains in the growth and stability of membrane nanotubes. *Blood Cells Mol Dis*. (2007) **39**:14–23. doi: 10.1016/j.bcmd.2007.02.013
19. Veksler A, Gov NS. Phase transitions of the coupled membrane-cytoskeleton modify cellular shape. *Biophys J*. (2007) **93**:3798–810. doi: 10.1529/biophysj.107.113282
20. Božič B, Kralj-Iglič V, Svetina S. Coupling between vesicle shape and lateral distribution of mobile membrane inclusions. *Phys Rev E*. (2006) **73**:041915. doi: 10.1103/PhysRevE.73.041915
21. Kozlov MM, Campelo F, Liska N, Chernomordik LV, Marrink SJ, McMahon HT. Mechanisms shaping cell membranes. *Curr Opin Cell Biol*. (2014) **29**:53–60. doi: 10.1016/j.ceb.2014.03.006
22. Boulbitch A. Deflection of a cell membrane under application of a local force. *Phys Rev E*. (1998) **57**:2123. doi: 10.1103/PhysRevE.57.2123
23. Evans E, Skalak R. *Mechanics and Thermodynamics of Biomembranes*. Boca Raton, FL: CRC Press (1980). doi: 10.1115/1.3138234
24. Mohandas N, Evans E. Mechanical properties of the red cell membrane in relation to molecular structure and genetic defects. *Annu Rev Biophys Biomol Struct*. (1994) **23**:787–818. doi: 10.1146/annurev.bb.23.060194.004035
25. Iglič A. A possible mechanism determining the stability of spiculated red blood cells. *J Biomech*. (1997) **30**:35–40. doi: 10.1016/S0021-9290(96)00100-5
26. Iglič A, Kralj-Iglič V, Hägerstrand H. Amphiphile induced echinocyte-spheroechinocyte transformation of red blood cell shape. *Eur Biophys J*. (1998) **27**:335–9. doi: 10.1007/s002490050140
27. Lim HWG, Wortis M, Mukhopadhyay R. Stomatocyte-discocyte-echinocyte sequence of the human red blood cell: evidence for the bilayer-couple hypothesis from membrane mechanics. *Proc Natl Acad Sci USA*. (2002) **99**:16766–9. doi: 10.1073/pnas.202617299
28. Rodríguez-García R, López-Montero I, Mell M, Egea G, Gov NS, Monroy F. Direct cytoskeleton forces cause membrane softening in red blood cells. *Biophys J*. (2015) **108**:2794–806. doi: 10.1016/j.bpj.2015.05.005
29. Smith AS, Nowak RB, Zhou S, Giannetto M, Gokhin DS, Papoin J, et al. Myosin IIA interacts with the spectrin-actin membrane skeleton to control red blood cell membrane curvature and deformability. *Proc Natl Acad Sci USA*. (2018) **115**:E4377–85. doi: 10.1073/pnas.1718285115
30. Alimohamadi H, Smith AS, Nowak RB, Fowler VM, Rangamani P. Non-uniform distribution of myosin-mediated forces governs red blood cell membrane curvature through tension modulation. *PLoS Comput Biol*. (2020) **16**:e1007890. doi: 10.1371/journal.pcbi.1007890
31. Penič S, Fošnarič M, Iglič A, Kralj-Iglič V. Active forces of myosin motors may control the endovesiculation of red blood cells. *Acta Chim Sloven*. (2020) **37**:674–81. doi: 10.17344/acsi.2020.5863
32. Graziano BR, Town JP, Sitarska E, Nagy TL, Fošnarič M, Penič S, et al. Cell confinement reveals a branched-actin independent circuit for neutrophil polarity. *PLoS Biol*. (2019) **17**:e3000457. doi: 10.1371/journal.pbio.3000457
33. Mukhopadhyay R, Lim HG, Wortis M. Echinocyte shapes: bending, stretching, and shear determine spicule shape and spacing. *Biophys J*. (2002) **82**:1756–72. doi: 10.1016/S0006-3495(02)75527-6
34. Sheetz MP, Singer S. Biological membranes as bilayer couples. A molecular mechanism of drug-erythrocyte interactions. *Proc Natl Acad Sci USA*. (1974) **71**:4457–61. doi: 10.1073/pnas.71.11.4457
35. Hägerstrand H, Isomaa B. Morphological characterization of exovesicles and endovesicles released from human erythrocytes following treatment with amphiphiles. *Biochim Biophys Acta*. (1992) **1109**:117–26. doi: 10.1016/0005-2736(92)90074-V
36. Hägerstrand H, Isomaa B. Vesiculation induced by amphiphiles in erythrocytes. *Biochim Biophys Acta*. (1989) **982**:179–86. doi: 10.1016/0005-2736(89)90053-9
37. Kralj-Iglič V, Hägerstrand H, Veranič P, Jezernik K, Babnik B, Gauger DR, et al. Amphiphile-induced tubular budding of the bilayer membrane. *Eur Biophys J*. (2005) **34**:1066–70. doi: 10.1007/s00249-005-0481-0
38. Deuticke B. Transformation and restoration of biconcave shape of human erythrocytes induced by amphiphilic agents and changes of ionic environment. *Biochim Biophys Acta*. (1968) **163**:494–500. doi: 10.1016/0005-2736(68)90078-3
39. Helfrich W. Blocked lipid exchange in bilayers and its possible influence on the shape of vesicles. *Z Naturforsch C*. (1974) **29**:510–5. doi: 10.1515/znc-1974-9-1010
40. Stokke B, Mikkelsen A, Elgsaeter A. The human erythrocyte membrane skeleton may be an ionic gel. *Eur Biophys J*. (1986) **13**:203–18. doi: 10.1007/BF00260368
41. Evans EA. Bending resistance and chemically induced moments in membrane bilayers. *Biophys J*. (1974) **14**:923–31. doi: 10.1016/S0006-3495(74)85959-X
42. Brochard F, Lennon JF. Frequency spectrum of the flicker phenomenon in erythrocytes. *J Phys*. (1975) **36**:1035–47. doi: 10.1051/jphys:019750036011010350O
43. Miao L, Seifert U, Wortis M, Döbereiner HG. Budding transitions of fluid-bilayer vesicles: the effect of area-difference elasticity. *Phys Rev E*. (1994) **49**:5389. doi: 10.1103/PhysRevE.49.5389
44. Deuling H, Helfrich W. The curvature elasticity of fluid membranes: a catalogue of vesicle shapes. *J Phys*. (1976) **37**:1335–45. doi: 10.1051/jphys:019760037011013350O
45. Evans E. Bending elastic modulus of red blood cell membrane derived from buckling instability in micropipet aspiration tests. *Biophys J*. (1983) **43**:27. doi: 10.1016/S0006-3495(83)84319-7
46. Geekiyanage NM, Balanant MA, Sauret E, Saha S, Flower R, Lim CT, et al. A coarse-grained red blood cell membrane model to study stomatocyte-discocyte-echinocyte morphologies. *PLoS ONE*. (2019) **14**:e215447. doi: 10.1371/journal.pone.0215447
47. Muñnoz S, Sebastián J, Sancho M, Álvarez G. Elastic energy of the discocyte-stomatocyte transformation. *Biochim Biophys Acta*. (2014) **1838**:950–6. doi: 10.1016/j.bbamem.2013.10.020
48. Iglič A, Svetina S, Žekš B. Depletion of membrane skeleton in red blood cell vesicles. *Biophys J*. (1995) **69**:274–9. doi: 10.1016/S0006-3495(95)79899-X
49. Hägerstrand H, Kralj-Iglič V, Bobrowska-Hägerstrand M, Iglič A. Membrane skeleton detachment in spherical and cylindrical microexovesicles. *Bull Math Biol*. (1999) **61**:1019–30. doi: 10.1006/bulm.1999.0128
50. Spangler EJ, Harvey CW, Revalee JD, Kumar PS, Laradji M. Computer simulation of cytoskeleton-induced blebbing in lipid membranes. *Phys Rev E*. (2011) **84**:051906. doi: 10.1103/PhysRevE.84.051906
51. Kralj-Iglič V, Iglič A, Hägerstrand H, Peterlin P. Stable tubular microexovesicles of the erythrocyte membrane induced by dimeric amphiphiles. *Phys Rev E*. (2000) **61**:4230. doi: 10.1103/PhysRevE.61.4230
52. Fait ME, Hermet M, Vazquez R, Mate S, Millone MAD, Vela ME, et al. Volume expansion of erythrocytes is not the only mechanism responsible for the protection by arginine-based surfactants against hypotonic hemolysis. *Colloids Surfaces B*. (2018) **171**:134–41. doi: 10.1016/j.colsurfb.2018.07.005
53. Kralj-Iglič V, Svetina S, Žekž B. Shapes of bilayer vesicles with membrane embedded molecules. *Eur Biophys J*. (1996) **24**:311–21. doi: 10.1007/BF00180372
54. Fischer TM. Bending stiffness of lipid bilayers. III. Gaussian curvature. *J Phys II*. (1992) **2**:337–43. doi: 10.1051/jp2:1992137
55. Fischer TM. Bending stiffness of lipid bilayers. V. Comparison of two formulations. *J Phys II*. (1993) **3**:1795–805. doi: 10.1051/jp2:1993230
56. Fournier J. Nontopological saddle-splay and curvature instabilities from anisotropic membrane inclusions. *Phys Rev Lett*. (1996) **76**:4436–39. doi: 10.1103/PhysRevLett.76.4436
57. Safinya C. Biomolecular materials: structure, interactions and higher order self-assembly. *Colloids Surfaces A*. (1997) **128**:183–95. doi: 10.1016/S0927-7757(96)03914-3
58. Fournier JB, Galatola P. Bilayer membranes with 2D-nematic order of the surfactant polar heads. *Braz J Phys*. (1998) **28**:8. doi: 10.1590/S0103-97331998000400008
59. Kralj-Iglič V. Stability of membranous nanostructures: a possible key mechanism in cancer progression. *Int J Nanomed*. (2012) **7**:3579. doi: 10.2147/IJN.S29076
60. Mesarec L, Góźdź W, Iglič A, Kralj-Iglič V, Virga E, Kralj S. Normal red blood cells' shape stabilized by membrane's in-plane ordering. *Sci Rep*. (2019) **9**:1–11. doi: 10.1038/s41598-019-56128-0
61. Bobrovska N, Góźdź W, Kralj-Iglič V, Iglič A. On the role of anisotropy of membrane components in formation and stabilization of tubular structures in multicomponent membranes. *PLoS ONE*. (2013) **8**:e73941. doi: 10.1371/journal.pone.0073941

62. Kabaso D, Lokar M, Kralj-Iglič V, Veranič P, Iglič A. Temperature and cholera toxin B are factors that influence formation of membrane nanotubes in RT4 and T24 urothelial cancer cell lines. *Int J Nanomed*. (2011) **6**:495. doi: 10.2147/IJN.S16982
63. Bobrowska-Hägerstrand M, Kralj-Iglič V, Iglič A, Bialkowska K, Isomaa B, Hägerstrand H. Torocyte membrane endovesicles induced by octaethyleneglycol dodecylether in human erythrocytes. *Biophys J*. (1999) **77**:3356–62. doi: 10.1016/S0006-3495(99)77167-5
64. Penič S, Iglič A, Bivas I, Fošnarič M. Bending elasticity of vesicle membranes studied by Monte Carlo simulations of vesicle thermal shape fluctuations. *Soft Matter*. (2015) **11**:5004–9. doi: 10.1039/C5SM00431D
65. Penič S, Perutková S, Fošnarič M, Iglič A. Monte Carlo methods used in inverted hexagonal lipid phase and in simulations of thermally fluctuating lipid vesicles. *Int J Adv Eng Sci Appl Math*. (2016) **8**:147–61. doi: 10.1007/s12572-016-0164-3
66. Helfrich W. Elastic properties of lipid bilayers: theory and possible experiments. *Z Naturforsch*. (1973) **28**:693–703. doi: 10.1515/znc-1973-11-1209
67. Bouvrais H. Bending rigidities of lipid bilayers: their determination and main inputs in biophysical studies. In: Iglič A, editor. Advances in Planar Lipid Bilayers and Liposomes, Vol. **15.** Cambridge: Elsevier (2012). p. 1–75. doi: 10.1016/B978-0-12-396533-2.00006-9
68. Dimova R. Recent developments in the field of bending rigidity measurements on membranes. *Adv Colloid Interface Sci*. (2014) **208**:225–34. doi: 10.1016/j.cis.2014.03.003
69. Mesarec L, Fošnarič M, Penič S, Kralj Iglič V, Kralj S, Góźdź W, et al. Numerical study of membrane configurations. *Adv Condens Matter Phys*. (2014) **2014**:373674. doi: 10.1155/2014/373674
70. Strey H, Peterson M, Sackmann E. Measurement of erythrocyte membrane elasticity by flicker eigenmode decomposition. *Biophys J*. (1995) **69**:478–88. doi: 10.1016/S0006-3495(95)79921-0
71. Betz T, Lenz M, Joanny JF, Sykes C. ATP-dependent mechanics of red blood cells. *Proc Natl Acad Sci USA*. (2009) **106**:15320–25. doi: 10.1073/pnas.0904614106
72. Yoon YZ, Hong H, Brown A, Kim DC, Kang DJ, Lew VL, et al. Flickering analysis of erythrocyte mechanical properties: dependence on oxygenation level, cell shape, and hydration level. *Biophys J*. (2009) **97**:1606–15. doi: 10.1016/j.bpj.2009.06.028
73. Park Y, Best CA, Auth T, Gov NS, Safran SA, Popescu G, et al. Metabolic remodeling of the human red blood cell membrane. *Proc Natl Acad Sci USA*. (2010) **107**:1289–94. doi: 10.1073/pnas.0910785107
74. Käs J, Sackmann E. Shape transitions and shape stability of giant phospholipid vesicles in pure water induced by area-to-volume changes. *Biophys J*. (1991) **60**:825–44. doi: 10.1016/S0006-3495(91)82117-8
75. Jesenek D, Perutková Š, Góźdź W, Kralj-Iglič V, Iglič A, Kralj S. Vesiculation of biological membrane driven by curvature induced frustrations in membrane orientational ordering. *Int J Nanomed*. (2013) **8**:677–87. doi: 10.2147/IJN.S38314
76. Kralj-Iglič V, Babnik B, Gauger DR, May S, Iglič A. Quadrupolar ordering of phospholipid molecules in narrow necks of phospholipid vesicles. *J Stat Phys*. (2006) **125**:727–52. doi: 10.1007/s10955-006-9051-9
77. MacKintosh F, Lubensky T. Orientational order, topology, and vesicle shapes. *Phys Rev Lett*. (1991) **67**:1169. doi: 10.1103/PhysRevLett.67.1169
78. Tian A, Baumgart T. Sorting of lipids and proteins in membrane curvature gradients. *Biophys J*. (2009) **96**:2676–88. doi: 10.1016/j.bpj.2008.11.067
79. Baumgart T, Capraro BR, Zhu C, Das SL. Thermodynamics and mechanics of membrane curvature generation and sensing by proteins and lipids. *Annu Rev Phys Chem*. (2011) **62**:483–506. doi: 10.1146/annurev.physchem.012809.103450
80. Iglič A, Drobne D, Kralj-Iglic V. *Nanostructures in Biological Systems: Theory and Applications*. New York, NY: Jenny Stanford Publishing (2015). doi: 10.1201/b18607
81. Zimmerberg J, Kozlov MM. How proteins produce cellular membrane curvature. *Nat Rev Mol Cell Biol*. (2006) **7**:9–19. doi: 10.1038/nrm1784
82. Gómez-Llobregat J, Elías-Wolff F, Lindén M. Anisotropic membrane curvature sensing by amphipathic peptides. *Biophys J*. (2016) **110**:197–204. doi: 10.1016/j.bpj.2015.11.3512
83. Helfrich W, Prost J. Intrinsic bending force in anisotropic membranes made of chiral molecules. *Phys Rev A*. (1988) **38**:3065. doi: 10.1103/PhysRevA.38.3065
84. Oda R, Huc I, Schmutz M, Candau S, MacKintosh F. Tuning bilayer twist using chiral counterions. *Nature*. (1999) **399**:566–9. doi: 10.1038/21154
85. Koehler S, Schaller V, Bausch AR. Collective dynamics of active cytoskeletal networks. *PLoS ONE*. (2011) **6**:e23798. doi: 10.1371/journal.pone.0023798
86. Bacia K, Schwille P, Kurzchalia T. Sterol structure determines the separation of phases and the curvature of the liquid-ordered phase in model membranes. *Proc Natl Acad Sci USA*. (2005) **102**:3272–7. doi: 10.1073/pnas.0408215102
87. Lubensky T, Prost J. Orientational order and vesicle shape. *J Phys II*. (1992) **2**:371–82. doi: 10.1051/jp2:1992133
88. Watson MC, Penev ES, Welch PM, Brown FL. Thermal fluctuations in shape, thickness, and molecular orientation in lipid bilayers. *J Chem Phys*. (2011) **135**:244701. doi: 10.1063/1.3660673
89. Kamien RD. The geometry of soft materials: a primer. *Rev Modern Phys*. (2002) **74**:953. doi: 10.1103/RevModPhys.74.953
90. Kralj S, Rosso R, Virga EG. Curvature control of valence on nematic shells. *Soft Matter*. (2011) **7**:670–83. doi: 10.1039/C0SM00378F
91. Mermin ND. The topological theory of defects in ordered media. *Rev Modern Phys*. (1979) **51**:591. doi: 10.1103/RevModPhys.51.591
92. Kurik MV, Lavrentovich O. Defects in liquid crystals: homotopy theory and experimental studies. *Soviet Phys Uspekhi*. (1988) **31**:196. doi: 10.1070/PU1988v031n03ABEH005710
93. Jesenek D, Perutková Š, Kralj-Iglič V, Kralj S, Iglič A. Exocytotic fusion pore stability and topological defects in the membrane with orientational degree of ordering. *Cell Calcium*. (2012) **52**:277–82. doi: 10.1016/j.ceca.2012.04.001
94. Mesarec L, Góźdź W, Iglič A, Kralj S. Effective topological charge cancelation mechanism. *Sci Rep*. (2016) **6**:27117. doi: 10.1038/srep27117
95. Bowick M, Nelson DR, Travesset A. Curvature-induced defect unbinding in toroidal geometries. *Phys Rev E*. (2004) **69**:041102. doi: 10.1103/PhysRevE.69.041102
96. Vitelli V, Turner AM. Anomalous coupling between topological defects and curvature. *Phys Rev Lett*. (2004) **93**:215301. doi: 10.1103/PhysRevLett.93.215301
97. Kurioz P, Mesarec L, Iglič A, Kralj S. Assembling of topological defects at neck-shaped membrane parts. *Phys Status Solidi*. (2019) **216**:1800722. doi: 10.1002/pssa.201800722
98. Rosso R, Virga EG, Kralj S. Parallel transport and defects on nematic shells. *Contin Mech Thermodyn*. (2012) **24**:643–64. doi: 10.1007/s00161-012-0259-4
99. Mesarec L, Kurioz P, Iglič A, Góźdź W, Kralj S. Curvature-controlled topological defects. *Crystals*. (2017) **7**:153. doi: 10.3390/cryst7060153
100. Lavrentovich OD. Topological defects in dispersed liquid crystals, or words and worlds around liquid crystal drops. *Liquid Cryst*. (1998) **24**:117–26. doi: 10.1080/026782998207640
101. Fischer TM. Bending stiffness of lipid bilayers. II. Spontaneous curvature of the monolayers. *J Phys II*. (1992) **2**:327–36. doi: 10.1051/jp2:1992129
102. Fischer TM. Mechanisms for determining the time scales in vesicle budding. *Phys Rev E*. (1994) **50**:4156. doi: 10.1103/PhysRevE.50.4156
103. Veranič P, Lokar M, Schütz GJ, Weghuber J, Wieser S, Hägerstrand H, et al. Different types of cell-to-cell connections mediated by nanotubular structures. *Biophys J*. (2008) **95**:4416–25. doi: 10.1529/biophysj.108.131375
104. Mathivet L, Cribier S, Devaux PF. Shape change and physical properties of giant phospholipid vesicles prepared in the presence of an AC electric field. *Biophys J*. (1996) **70**:1112–21. doi: 10.1016/S0006-3495(96)79693-5
105. Kralj-Iglič V, Iglič A, Gomišček G, Sevšek F, Arrigler V, Hägerstrand H. Microtubes and nanotubes of a phospholipid bilayer membrane. *J Phys A*. (2002) **35**:1533. doi: 10.1088/0305-4470/35/7/305
106. Napoli G, Vergori L. Extrinsic curvature effects on nematic shells. *Phys Rev Lett*. (2012) **108**:207803. doi: 10.1103/PhysRevLett.108.207803

Conflict of Interest: The authors declare that the research was conducted in the absence of any commercial or financial relationships that could be construed as a potential conflict of interest.